ACI MATERIALS JOURNAL TECHNICAL PAPER

Title no. 93-M38

Carbon Fiber Reinforced Concrete as an Intrinsically Smart Concrete for Damage Assessment during Static and Dynamic Loading

by Pu-Woei Chen and D. D. L. Chung

Concrete containing short carbon fibers (in amounts as small as 0.2 volume-percent) was found to be an intrinsically smart concrete that can sense elastic deformation, inelastic deformation, and fracture. The signal provided is the change in electrical resistance, which is reversible for elastic deformation and irreversible for inelastic deformation and fracture. The presence of electrically conducting short fibers is necessary for the concrete to sense elastic or inelastic deformation, but the sensing of fracture does not require fibers. The fibers serve to bridge the cracks and provide a conduction path. The resistance increase is due to conducting fiber pullout in the elastic regime, conducting fiber breakage in the inelastic regime, and crack propagation at fracture. Applications include real-time damage assessment and dynamic load monitoring.

Keywords: carbon; concretes; damage; dynamic loads; electrical resistance; fibers.

INTRODUCTION

Smart structures capable of nondestructive health monitoring (damage assessment) in real time are of increasing importance due to the need to maintain the functions of critical civil infrastructure systems. Structures in earthquake-prone regions are in particular need of in situ health monitoring.

The sensing function refers to the ability to provide an electrical or optical response to damage such as cracks in real time during dynamic loading. Requirements of the sensor include the following: 1) low cost for both materials and implementation; 2) durability and reliability; 3) measurement repeatability and stability; 4) ability to provide quantitative signals with high sensitivity and resolutions; 5) ability to provide spatial resolution (two- or three-dimensional); 6) fast response for real-time monitoring; 7) sensitivity to a wide dynamic range of strain, covering both the elastic and inelastic regimes of deformation; 8) not weakening the structure; 9) not requiring expensive peripheral equipment; and 10) applicability to both old and new structures.

Item No. 7 refers to the ability to detect and distinguish between inelastic deformation (which corresponds to permanent damage) and elastic deformation. This ability is valuable for monitoring damage occurrence during dynamic loading as it provides monitoring of the dynamic loading in its complete range, covering both the elastic and inelastic regimes. Thus, it allows determination of exactly in which part of which loading cycle damage occurs and does not require the load cycling to be periodic in time.

Item No. 5 refers to the ability to provide a measure of the degree and location of damage. This measure can be in terms of the inelastic strain, as strain in the inelastic regime is associated with damage. The greater the inelastic strain, the greater the damage. Due to the ability described in No. 7, the response due to the inelastic strain can be distinguished from that due to the elastic strain. Thus, the inelastic strain (or degree of damage) can be monitored in real time during dynamic loading.

Existing sensors include strain gages, optical fibers, and piezoelectric sensors. All such sensors suffer from their high cost and/or poor durability, poor sensitivity, undesirable frequency range, and the need for expensive peripheral equipment such as electronics and lasers. As a result, the use of sensors in civil structures is far from being common. New sensor technologies are badly needed.

RESEARCH SIGNIFICANCE

A new sensor technology had been developed by the authors.[1] In this technology, concrete itself is the sensor, so there is no need to embed strain gages, optical fibers, or other sensors in the concrete. This sensor satisfies all of the requirements listed previously. Moreover, the intrinsically smart concrete exhibits high flexural strength and toughness and low drying shrinkage.[2] In this paper, sensing ability and its origin are de-

ACI Materials Journal, V. 93, No. 4, July-August 1996.

Received Dec. 5, 1994, and reviewed under Institute publication policies. Pertinent discussion will be published in the May-June 1997 *ACI Materials Journal* if received by Feb. 1, 1997.

Pu-Woei Chen is a graduate student in the Department of Mechanical and Aerospace Engineering, State University of New York at Buffalo. He received his PhD degree from the State University of New York at Buffalo in 1994. His research interests include carbon fiber reinforced concrete.

D. D. L. Chung is a professor of mechanical and aerospace engineering, Niagara Mohawk Power Corp. Endowed Chair of Materials Research, and director of the Composite Materials Research Laboratory, State University of New York at Buffalo. She received her PhD in materials science from the Massachusetts Institute of Technology in 1977.

Table 1—Functions of intrinsically smart concrete

Application	Information sensed	Signal	Origin of signal
Dynamic load monitoring	Reversible strain	Reversible resistance change	Conducting fiber pullout
Damage assessment	Irreversible strain	Irreversible resistance change	Conducting fiber breakage
Damage assessment	Fracture	Irreversible, particularly large resistance change	Crack propagation

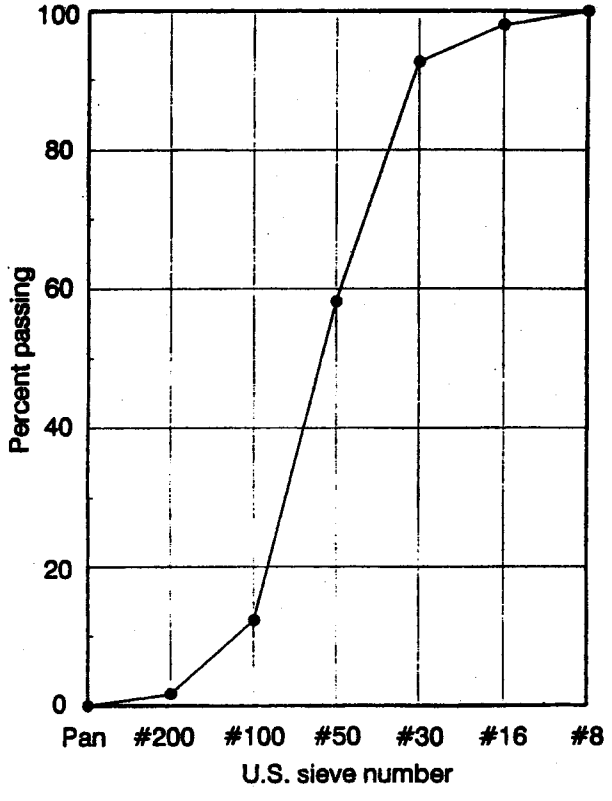

Fig. 1—Particle-size distribution of sand used

scribed systematically in relation to the sensing of elastic deformation, inelastic deformation, and fracture. In contrast to techniques such as acoustic emission, which cannot sense elastic deformation, this new sensor technology allows the sensing of elastic deformation in addition to inelastic deformation and fracture. The signal provided by this new sensor is the change in the electrical resistance. As summarized in Table 1, reversible strain is associated with reversible resistance change and irreversible strain is associated with irreversible resistance change, whereas fracture is associated with irreversible and particularly large resistance change. Thus, reversible and irreversible strains can be easily distinguished. The origin of the signal associated with fracture is crack propagation, which increases resistance due to the high resistivity of the cracks. The origin of the signal associated with irreversible strain is conducting fiber breakage; the origin of the signal associated with reversible strain is conducting fiber pullout. The detection of fracture does not require fibers in the concrete, whereas the detection of irreversible and reversible strains require the presence of short and electrically conducting fibers in the concrete. The evidences that support these origins are given in this paper.

Table 2—Properties of carbon fibers

Filament diameter	10 μm
Tensile strength	690 MPa
Tensile modulus	48 GPa
Elongation at break	1.4 percent
Electrical resistivity	3.0×10^{-3} Ω.cm
Specific gravity	1.6 g cm^{-3}
Carbon content	98 weight, percent

Table 3—List of raw materials

Material	Source
Type I portland cement	Lafarge Corp., Southfield, MI
TAMOL SN Sodium salt of condensed naphthalene-sulfonic acid, 93 to 96 percent Water, 51 to 54 percent	Rohm and Haas Co., Philadelphia, PA
Methocel, A15-LV Methylcellulose	Dow Chemical Corp., Midland, MI
Colloids 1010 Defoamer	Colloids, Inc., Marietta, GA
Latex 460NA Styrene butadiene, 40 to 60 percent Water, 40 to 60 percent Stabilizer, 1 to 5 percent	Dow Chemical Corp., Midland, MI
Antifoam 2410 Polydimethylsiloxane, 10 percent Water, preservatives, and emulsifiers, 90 percent	Dow Corning Corp., Midland, MI
Silica fume	Elkem Materials, Inc. Pittsburgh, PA
Carboflex Carbon fibers	Ashland Petroleum Co., Ashland, KY

EXPERIMENTAL

Raw materials

Unless noted otherwise, the fibers used were carbon fibers. They were short, isotropic pitch-based, and unsized. The nominal fiber length was 5 mm. The fiber properties are shown in Table 2. Fibers in the amount of 0.5 percent by weight of cement were used, unless stated otherwise. The aggregate used was natural sand, the particle-size analysis of which is shown in Fig. 1. Table 3 describes the various raw materials used. Table 4 describes the four types of mortar studied. They are: 1) plain mortar; 2) plain mortar with latex; 3) plain mortar with methylcellulose; and 4) plain mortar with methylcellulose and silica fume. The tensile specimens contained no sand due to their small cross-sectional area, whereas the compressive and flexural specimens contained sand. The latex, methylcellulose, and silica fume were added partly for the purpose of enhancing fiber dispersion, but in

Table 4—Mix proportions and electrical resistivity of various types of mortar

Test	Sample	Fiber volume, percent	Water/cement ratio	Sand/cement ratio	Latex/cement ratio	Meth*/cement, percent	SF†/cement ratio	WR‡/cement, percent	Electrical resistivity
Compressive	Plain mortar	0	0.45	1.5	0	0	0	0	1.46×10^5
	Plain mortar with latex	0 0.37	0.3 0.3	1.0 1.0	0.2 0.2	0 0	0 0	0 0	2.71×10^5 1.05×10^5
	Plain mortar with meth*	0 0.24	0.45 0.45	1.5 1.5	0 0	0.4 0.4	0 0	0 2	1.47×10^5 8.33×10^4
	Plain mortar with meth* and SF†	0 0.24	0.45 0.45	1.5 1.5	0 0	0.4 0.4	0.15 0.15	2 2	2.09×10^5 3.19×10^3
Tensile	Plain mortar	0	0.3	0	0	0	0	0.5	1.50×10^3
	Plain mortar with latex	0 0.53	0.23 0.23	0 0	0.2 0.2	0 0	0 0	0 0	2.75×10^5 9.87×10^5
	Plain mortar with meth*	0 0.53	0.32 0.32	0 0	0 0	0.4 0.4	0 0	0.5 1	1.49×10^5 2.53×10^4
	Plain mortar with meth* and SF†	0 0.53	0.35 0.35	0 0	0 0	0.4 0.4	0.15 0.15	3 3	2.32×10^5 2.14×10^3
Flexural	Plain mortar	0	0.475	1.0	0	0	0	0.5	1.46×10^5
	Plain mortar with latex	0 0.35	0.23 0.23	1.0 1.0	0.2 0.2	0 0	0 0	0.5 1.5	2.71×10^5 1.12×10^5
	Plain mortar with meth*	0 0.35	0.475 0.475	1.0 1.0	0 0	0.4 0.4	0 0	1 1	1.47×10^5 5.73×10^4
	Plain mortar with meth* and SF†	0 0.35	0.475 0.475	1.0 1.0	0 0	0.4 0.4	0.15 0.15	2 2	2.09×10^5 2.80×10^3

*Meth = methylcellulose.
†SF = silica fume.
‡WR = water-reducing agent.

each category such additives were used whether fibers were present or not to obtain the effect of the fiber addition alone. In addition, latex and silica fume served to enhance the fiber-matrix bonding.

The water-reducing admixture was 93 to 96 percent sodium salt of a condensed naphthalenesulfonic acid (TAMOL SN, Rohm and Haas). In general, the slump of carbon fiber reinforced cement tends to decrease with increasing carbon fiber content. Therefore, various amounts of this water-reducing admixture were used to maintain the mortar at a reasonable flow value in the range of 150 ± 50 mm.

The latex was a styrene butadiene polymer emulsion; it was used in the amount of 20 percent of the weight of the cement. The antifoam used was in the amount of 0.5 percent of the weight of the latex; it was used whenever latex was used.

Methylcellulose in the amount of 0.4 percent of the cement weight was used. The defoamer used along with it was in the amount of 0.13 volume-percent; it was used whenever methylcellulose was used.

Mixing procedure

A mixer with a rotating flat beater was used for mixing. For the case of mortar containing latex, the latex, antifoam, and carbon fibers first were mixed by hand for about 1 min. Then this mix, cement, sand, water, and the water-reducing admixture were mixed in the mixer for 5 min.

For the case of mortar containing methylcellulose, methylcellulose was dissolved in water. After that, the defoamer and then the fibers were added and stirred by hand for about 2 min. Then this mix, cement, sand, water, and water-reducing admixture (and silica fume, if applicable) were mixed in the mixer for 5 min.

For the case of concrete, only one formulation was used. This is the formulation involving methylcellulose and silica fume. The water-cement ratio was 0.50. The cement-fine aggregate-coarse aggregate ratio was 1:1.5:2.49 (by weight). The mixing procedure is quite similar to that for mortar containing methylcellulose and silica fume. Methylcellulose (0.4 percent by weight of cement) was dissolved in water. After that, the defoamer (0.13 volume-percent) and then the fibers (0.5 percent by weight of cement) were added and stirred by hand for about 2 min. Then this mix, cement (portland cement, Type I), fine aggregate (Aggregate B described in Reference 2, 100 percent passing through #4 U.S. sieve), silica fume (15 percent by weight of cement), and then the water-reducing admixture (2 percent by weight of cement) were mixed in the mixer for 5 min. Subsequently, the mix was placed in a stone concrete mixer to which the coarse aggregate (Aggregate D described in Reference 2, 100 percent passing through 1-in. U.S. sieve) was added and then mixing was conducted for about 3 min. After casting the mix into oiled molds, a vibrator was used to compact.

Curing procedure

The specimens were demolded after 1 day and then allowed to cure at room temperature in air for 7 days. Regular room humidity (about 50 percent relative humidity) was used.

Testing procedure

The specimen dimensions depended on the deformation mode—compressive, tensile, or flexural. They are all in accordance with ASTM standards for mortars or concretes.

For compressive testing according to ASTM C 109-80, mortar specimens were prepared by using a 2 x 2 x 2-in. (5.1 x

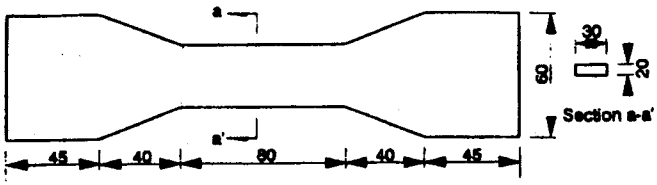

Fig. 2—Shape and dimensions (in mm) of specimens tested under tension

5.1 x 5.1-cm) mold. For compressive testing according to ASTM C 39-83b, concrete specimens were prepared using a 4-in.-diameter x 8-in.-length (102-mm-diameter x 203-mm-length) mold. Compression testing was performed using a hydraulic material testing system (MTS). The displacement rate was 1.27 mm/min, unless noted otherwise.

Dog bone-shaped specimens of the dimensions shown in Fig. 2 were used for tensile testing. They were prepared by using molds of the same shape and size. Tensile testing was performed using a screw type mechanical testing system. The displacement rate was 1.27 mm/min, unless noted otherwise.

During compressive or tensile loading up to fracture, the strain was measured by the crosshead displacement in compressive testing or by a strain gage in tensile testing, while the fractional change in electrical resistance was measured using the four-probe method. The resistance was measured along the stress axis. The electrical contacts were made by silver paint applied along the whole perimeter in four parallel planes perpendicular to the stress axis. The inner two contacts were for voltage measurement, while the outer two contacts were for passing a current. Although the spacing between the contacts increased on tensile deformation and decreased on compressive deformation, the increase was so small that the measured resistance remained essentially proportional to the volume resistivity. Testing was performed either in one cycle up to the breaking stress or in multiple cycles on loading up to a fraction ($^1/_3$ under compression and ~ $^1/_2$ under tension) of the breaking stress.

Flexural testing was performed by three-point bending (ASTM C 348-80), with a span of 140 mm (5.5 in.). The specimen size was 40 x 40 x 160 mm. Flexural testing was performed using a screw type mechanical testing system. The displacement rate was 1.27 mm/min. During flexural loading up to fracture, the fractional change in electrical resistance was measured separately at the top surface (side under compression) and the bottom surface (side under tension). Electrical contacts were made by silver paint applied along four parallel lines (perpendicular to the long axis of the specimen) on each of the two opposite surfaces of the specimen. Resistance measurements were all made at a DC current in the range from 0.1 to 4 A. For all the tests, six specimens of each type were used.

Results

Table 5 summarizes the results of simultaneous compressive/tensile/flexural testing and electrical resistivity measurement along the stress axis. The mechanical testing results include the ultimate strength and ductility. The electrical probing gave as raw result the resistance R between the two voltage probes in the four-probe setup. Table 5 gives the fractional change in R at the point of fracture, i.e., $\Delta R/R_o$, where R_o is the original resistance. The resistivity ρ is related to the resistance R by the equation

$$\rho = R\frac{A}{d} \quad (1)$$

where A is the cross-sectional area and d is the distance between the voltage probes. For compressive testing, d = 1 cm and 4 in. for mortars and concretes, respectively; for tensile testing, d = 4 cm (for mortars only); for flexural testing, d = 8 cm (for mortars only). As the dimensional changes are small during the deformation up to fracture, the fractional change in the electrical resistivity (i.e., $\Delta\rho/\rho_o$, where ρ_o is the original resistivity) is almost the same as $\Delta R/R_o$. For tensile and flexural testing, $\Delta R/R_o$ exactly equals $\Delta\rho/\rho_o$ because of the low ductility under tension or flexure. For compressive testing, $\Delta\rho/\rho_o$ is slightly larger than $\Delta R/R_o$. For example, $\Delta R/R_o$ values of 4.1, 10.42, and 21.14 correspond to $\Delta\rho/\rho_o$ values of

Table 5—Results of simultaneous compressive/tensile/flexural testing and electrical resistivity measurement along stress axis

	Compressive			Tensile			Flexural		
	Strength, MPa	Ductility, percent	$\Delta R/R_o$*	Strength, MPa	Ductility, percent	$\Delta R/R_o$*	Strength, MPa	Ductility, percent	$\Delta R/R_o$*†
Plain mortar	35.6	0.16	69.5	0.88	0.004	0.88	3.64	0.002	0.59/0.72
L	38.6	0.24	30	3.03	0.0352	0.6	5.99	0.003	0.21/0.70
L + 0.37 volume-percent F	37.8	0.17	4.1	—	—	—	—	—	—
L + 0.53 volume-percent F	—	—	—	3.15	0.0413	0.053	—	—	—
L + 0.35 volume-percent F	—	—	—	—	—	—	8.64	0.006	0.136/0.058
M	34.5	0.17	3.4	1.37	0.0209	0.18	3.43	0.005	1.76/0.55
M + 0.24 volume-percent F	33.6	0.15	10.42	—	—	—	—	—	—
L + 0.53 volume-percent F	—	—	—	1.95	0.0192	0.034	—	—	—
L + 0.35 volume-percent F	—	—	—	—	—	—	4.97	0.009	0.184/0.126
M + SF	42.7	0.16	9.7	0.83	0.088	0.037	3.94	0.002	0.67/0.32
M + SF + 0.24 volume-percent F	41.0	0.19	21.14	—	—	—	—	—	—
M + SF + 0.53 volume-percent F	—	—	—	1.88	0.0173	0.051	—	—	—
M + SF + 0.35 volume-percent F	—	—	—	—	—	—	5.11	0.004	0.121/0.104

*At fracture.
†Under compression/tension.
Note: L = latex
M = methylcellulose
SF = silica fume
F = fibers

Table 6—Results of simultaneous tensile testing and electrical resistivity measurement

		L			M			M + SF		
Sample	Fiber/cement ratio	$\Delta R/R_o$*	ρ_o (Ωcm)	Strength, MPa	$\Delta R/R_o$*	ρ_o (Ωcm)	Strength, MPa	$\Delta R/R_o$*	ρ_o (Ωcm)	Strength, MPa
Plain mortar	0	0.88	1.50×10^5	0.88	0.88	1.50×10^5	0.88	0.88	1.50×10^5	0.88
(+ L)/(+ M)/(+ M + SF)	0	0.6	2.75×10^5	3.03	0.18	1.49×10^5	1.37	0.037	2.32×10^5	0.83
+ 0.53 volume-percent F	0.5 percent	0.053	9.87×10^4	3.15	0.034	2.53×10^4	1.95	0.051	2.14×10^3	1.88
+ 1.06 volume-percent F	1.0 percent	0.057	119	3.16	0.027	26.1	2.61	0.048	13.9	2.03
+ 2.12 volume-percent F	2.0 percent	0.048	19.7	3.65	0.033	16.9	3.05	0.063	5.02	2.84
+ 3.18 volume-percent F	3.0 percent	0.061	12.2	3.32	0.041	7.82	2.97	0.057	3.88	3.01
+ 4.24 volume-percent F	4.0 percent	0.047	7.96	2.92	0.043	2.84	2.65	0.055	3.58	2.49

*At fracture.
Note: L = latex
M = methylcellulose
SF = silica fume
F = fibers

4.1, 10.44, and 21.18, respectively. The quantity $\Delta R/R_o$ is useful to field application of this in situ health monitoring technique. The quantity $\Delta\rho/\rho_o$ is more meaningful scientifically.

In compressive, tensile, and flexural cases, $\Delta R/R_o$ is positive, i.e., the resistivity increases as deformation takes place. This is because flaws are generated as deformation occurs. However, $\Delta R/R_o$ at fracture is much larger under compression than under tension or flexure. This is due to the much higher ductility under compression than under tension or flexure. In all cases where the mortar contains no fibers, $\Delta R/R_o$ varies randomly with strain/stress up to fracture, at which $\Delta R/R_o$ abruptly increases.

Simultaneous tensile testing and electrical resistivity measurement along the stress axis were conducted on mortars with fiber volume fractions 0.53, 1.06, 2.12, 3.18, and 4.24 percent (corresponding to fibers in amounts of 0.5, 1.0, 2.0, 3.0, and 4.0 percent of the cement weight). The results are shown in Table 6. The tensile strength increased with increasing fiber content up to 2.12 percent for the cases of mortars with latex or methylcellulose and 3.18 percent for the case of mortar with methylcellulose and silica fume. Above these fiber contents, the tensile strength decreased due to the decreased workability and the resulting higher void content. The value of $\Delta R/R_0$ did not vary much with the fiber content (Table 6), even though the value of ρ_0 decreased significantly with increasing fiber content (Table 6 and Fig. 3). This means that a very low electrical resistivity is not required for the smart behavior to occur; a low value of ρ_0 does not result in a large value of $\Delta R/R_0$.

Fig. 4 through 6 give the plot of $\Delta R/R_0$ versus strain (or displacement in the case of flexural loading), together with the simultaneously obtained plot of stress versus strain (or displacement in the case of flexural loading) for compressive, tensile, and flexural loading, respectively, for mortars containing methylcellulose and fibers. The ductility values in Table 5 correspond to the strains at failure or the strains at the maximum stress in Fig. 4 through 6. In the case of flexural loading, $\Delta R/R_0$ is given for the side of the specimen under compression as well as the side of the specimen under tension; $\Delta R/R_0$ is larger for the side under compression. Fig. 7 gives the corresponding plot for plain mortar (without any dispersant or fiber) under compression; prior to fracture, $\Delta R/R_0$ has no correlation with strain/stress (with only noise observed) when fibers were absent.

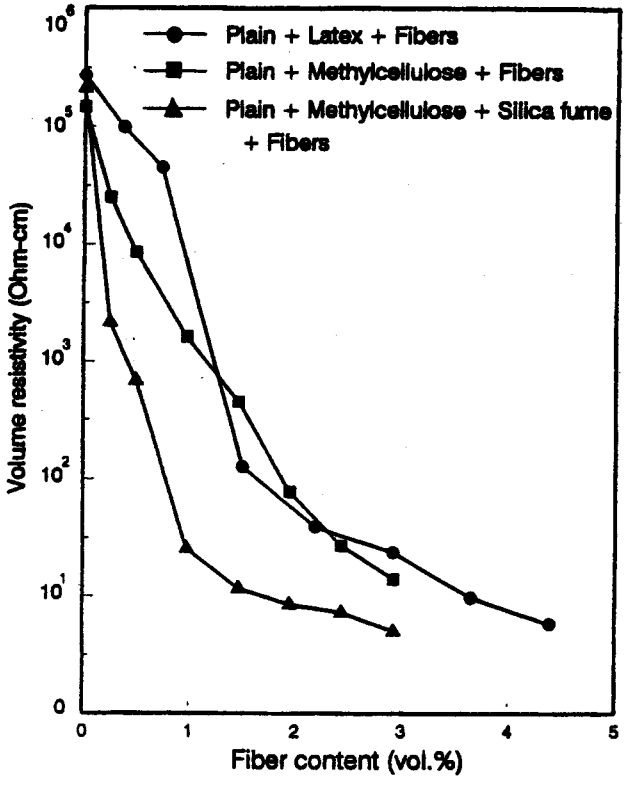

Fig. 3—Volume electrical resistivity versus carbon fiber volume fraction for mortars containing: (a) latex; (b) methylcellulose; (c) methylcellulose + silica fume

All the smart performance results given previously were obtained during static loading. Consistent results were obtained under cyclic compressive/tensile loading, as described below. Without fibers, no smart action was observed at all. With fibers and methylcellulose, the smart behavior was as shown in Fig. 8 and 9 for cyclic compressive and cyclic tensile loading, respectively. Under cyclic compressive loading within the regime where the strain was essentially fully reversible (Fig. 8), the smart action was observed as 1) irreversibly increasing $\Delta R/R_o$ during the first loading, 2) reversibly increasing $\Delta R/R_o$ during unloading in any cycle, and 3) reversibly decreasing $\Delta R/R_o$ during the second and subsequent loadings. The irreversibly increasing $\Delta R/R_o$ during the first loading (which involved no irreversible

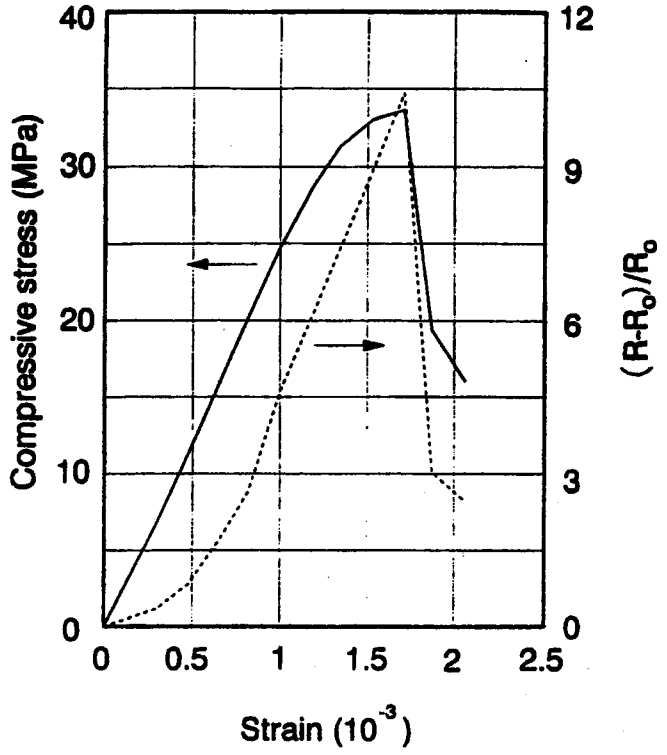

Fig. 4—Plot of $\Delta R/R_o$ versus strain (dashed curve) and plot of stress versus strain (solid curve) during static compressive testing for mortar containing methylcellulose and 0.24 volume-percent fibers

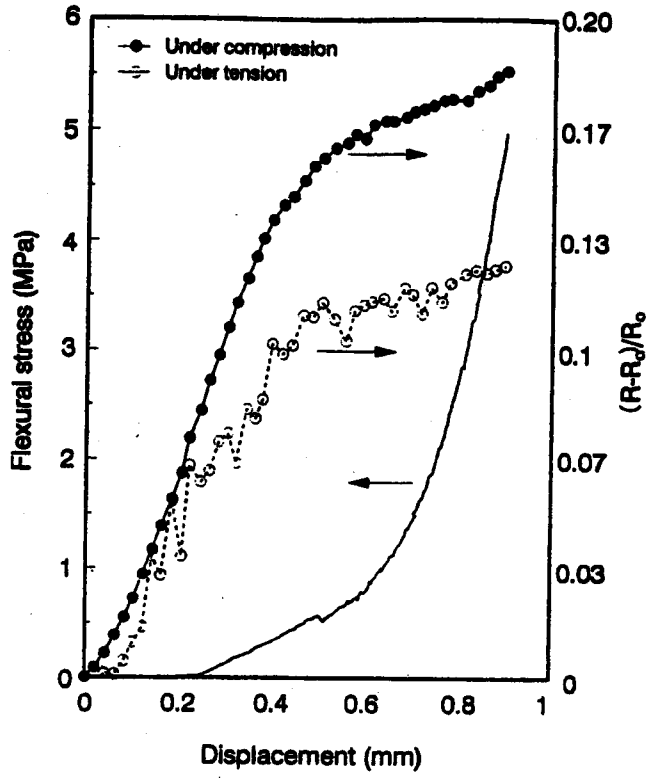

Fig. 6—Plots of $\Delta R/R_o$ (at compression side and tension side of specimen) versus displacement (solid and open circles, respectively) and plot of stress versus displacement (solid curve without circles) during static flexural testing for mortar containing methylcellulose and 0.35 volume-percent fibers

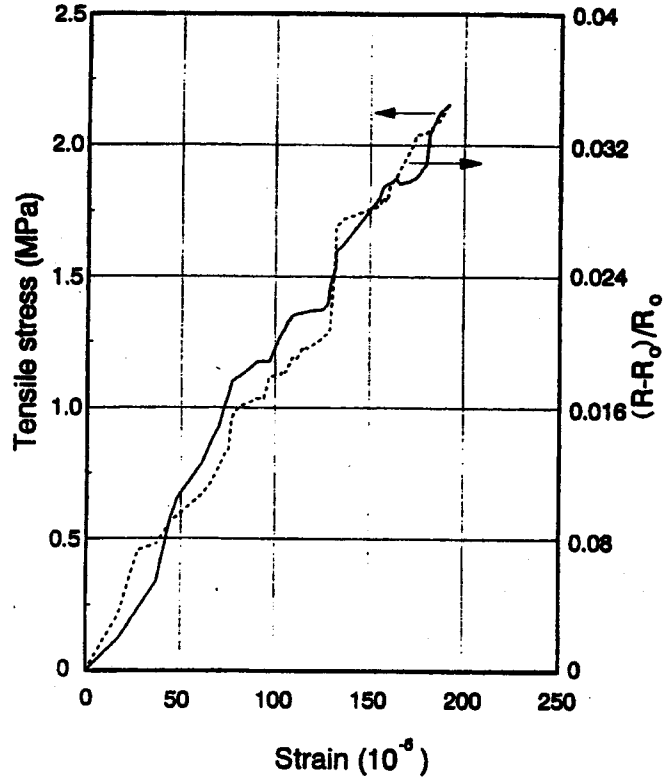

Fig. 5—Plot of $\Delta R/R_o$ versus strain (dashed curve) and plot of stress versus strain (solid curve) during static tensile testing for mortar containing methylcellulose and 0.53 volume-percent fibers

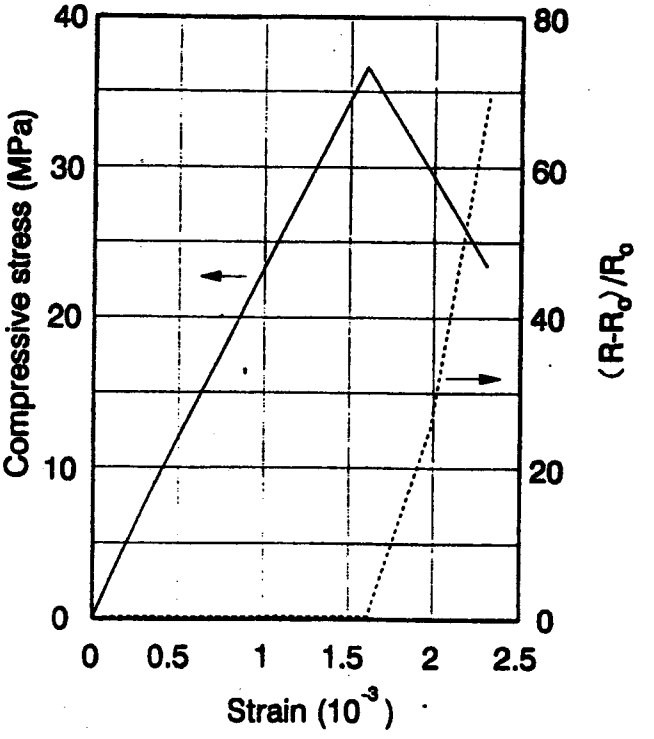

Fig. 7—Plot of $\Delta R/R_o$ versus strain (dashed curve) and plot of stress versus strain (solid curve) during static compressive testing for plain mortar

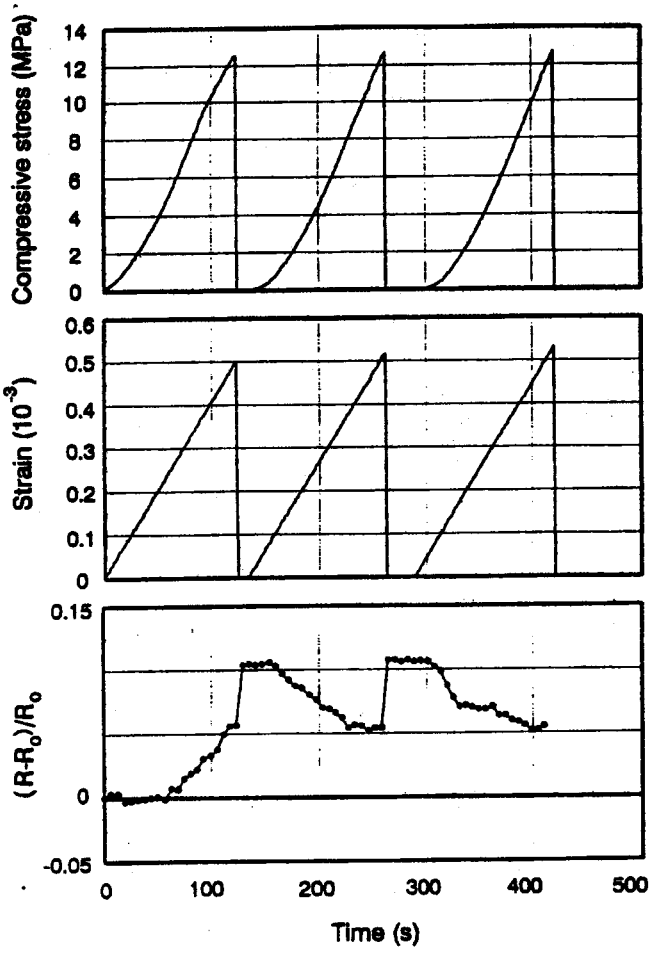

Fig. 8—Plots versus time of $\Delta R/R_o$, compressive strain, and compressive stress obtained during cyclic compressive testing for mortar containing methylcellulose and 0.24 volume-percent fibers

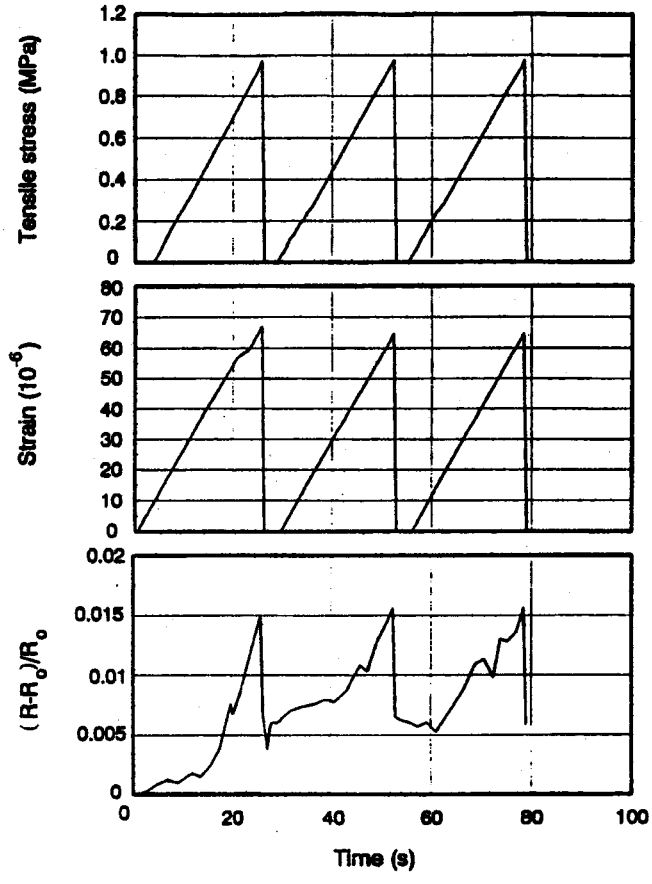

Fig. 9—Plots versus time of $\Delta R/R_o$, tensile strain, and tensile stress obtained during cyclic tensile testing for mortar containing methylcellulose and 0.53 volume-percent fibers

strain) is attributed to the irreversible increase in the contact electrical resistivity at the fiber-matrix interface due to the weakening of that interface. Note that the increase in $\Delta R/R_o$ during first loading cannot be explained by the fibers becoming closer together, as increased proximity of adjacent fibers will decrease R rather than increasing R. The irreversibly changed $\Delta R/R_o$ provides a memory indicating that prior loading has occurred. The reversibly increasing $\Delta R/R_o$ during unloading in any cycle is attributed to crack opening (i.e., increase in the length and/or height of a crack), which was hindered under compressive loading. The reversibly decreasing $\Delta R/R_o$ during the second and subsequent loadings is attributed to the crack closure (i.e., decrease in the length or height of a crack) under compressive loading. The reversibility of the crack opening and closing is attributed to the fiber bridging across the crack, with fiber pullout occurring during crack opening and fiber push-in occurring during crack closing. The occurrence of fiber pullout requires a relatively weak fiber-matrix interface, which is provided by the interface weakening associated with the irreversible increase in $\Delta R/R_o$ prior to the fiber pullout or crack opening.

Under cyclic tensile loading within the regime where the strain was fully reversible (Fig. 9), the smart action was observed as 1) irreversibly increasing $\Delta R/R_o$ during the initial portion of the first loading, 2) reversibly increasing $\Delta R/R_o$ during the latter portion of the first loading and during any subsequent loading, and 3) reversibly decreasing $\Delta R/R_o$ during unloading in any cycle. The increase in $\Delta R/R_o$ during loading is attributed to crack opening, whereas the decrease in $\Delta R/R_o$ during unloading is attributed to crack closure. That the initial portion of the first loading exhibited irreversibly increasing $\Delta R/R_o$ whereas the latter portion was reversible is because the irreversible part is due to the fiber-matrix interface weakening, whereas the reversible part is due to crack opening. The stress at which the irreversible increase in $\Delta R/R_o$ starts to occur is the stress at which the fiber-matrix interface weakening starts to occur, whereas the stress at which the irreversible $\Delta R/R_o$ increase ends and the reversible $\Delta R/R_o$ increase starts is the stress at which the fiber-matrix interface is sufficiently weak for it to not restrain crack opening or fiber pullout. The cracks under tension were preferentially oriented perpendicular to the stress axis.

Under both cyclic compression and cyclic tension, the stress/strain at which the irreversible $\Delta R/R_o$ increase starts to occur is the stress/strain at which the fiber-matrix interface weakening starts to occur. Table 7 lists these stress/strain values under compression and tension for the three formulations of carbon fiber reinforced mortars.

All the data given previously were obtained on mortars. Consistent results were obtained on concretes. Table 8 lists the values of $\Delta R/R_o$ (at compressive fracture) and ρ_o for mortars and concretes containing 0.2 volume-percent fibers. At the same fiber volume fraction, ρ_o is much higher for concrete

Table 7—Stress and strain at which irreversible increase in $\Delta R/R_o$ starts to occur

	Stress, MPa	Strain
Compression		
L + 0.37 volume-percent F	0.03	1.6×10^{-5}
M + 0.24 volume-percent F	0.35	2.5×10^{-5}
M + SF + 0.24 volume-percent F	0.29	9.7×10^{-5}
Tension		
L + 0.53 volume-percent F	0.001	2×10^{-8}
M + 0.53 volume-percent F	0.004	5.7×10^{-7}
M + SF + 0.53 volume-percent F	0.063	2.9×10^{-7}

Note: L = latex
M = methylcellulose
SF = silica fume
F = fibers

Table 8—$\Delta R/R_o$ at compressive fracture and ρ_o for mortars and concretes containing 0.2 volume-percent carbon fibers

	$\Delta R/R_o$		ρ_o (Ωcm)	
Dispersant	Mortar*	Concrete†	Mortar*	Concrete†
Methylcellulose	10.42	0.37	8.33×10^4	3.70×10^6
Methylcellulose + silica fume	21.14	0.105	3.19×10^3	2.32×10^6

*0.24 volume-percent carbon fibers.
†0.19 volume-percent carbon fibers.

than mortar. In spite of the high ρ_o for carbon fiber reinforced concretes (even higher than those of plain mortars exhibiting no smart action [Table 4]), the smart action occurred, indicating that the occurrence of smart action is not governed by ρ_o. This means that the low $\Delta R/R_o$ of concretes is not due to the high ρ_o, but rather is due to the presence of the coarse aggregate, which makes the cracking control ability of the fibers less prominent. In spite of the low values of $\Delta R/R_o$ for concretes, the measurement of $\Delta R/R_o$ was not difficult, even at the lowest fiber content of 0.19 volume-percent.

The fractions $(\Delta R/R_o)_{reversible}/(\Delta R/R_o)_{fracture}$ and $(\Delta R/R_o)_{irreversible}/(\Delta R/R_o)_{fracture}$ vary with the stress amplitude in cyclic loading, as shown in Table 9, where the stress amplitude is expressed as the maximum stress divided by the fracture stress. The fractions listed are for compression of mortars containing latex and 0.37 volume-percent carbon fibers. They increase with increasing stress amplitude, such that they are much larger when the stress amplitude is 0.50 than when the stress amplitude is 0.33 or below. This is attributed to the abrupt increase in crack concentration or size when the stress is increased from 0.33 to 0.50 of the fracture stress. The fraction $(\Delta R/R_o)_{reversible}/(\Delta R/R_o)_{fracture}$ increases most abruptly as the stress amplitude is increased from 0.40 to 0.50, whereas the fraction $(\Delta R/R_o)_{irreversible}/(\Delta R/R_o)_{fracture}$ increases most abruptly as the stress amplitude is increased from 0.33 to 0.40. The ratio of the reversible part of $\Delta R/R_o$ to the irreversible part of $\Delta R/R_o$ is smaller at a stress amplitude of 0.40 or above compared to those at lower stress amplitudes because the abrupt increase in crack concentration or size when the stress is increased from 0.33 to 0.40 of the fracture stress is due mainly to irreversible cracking rather than reversible cracking. The ratio of the reversible part of $\Delta R/R_o$ to the irreversible part of $\Delta R/R_o$ is largest at a stress amplitude of 0.33 and decreases slightly with decreasing stress amplitude below 0.33, probably because there is a minimum amount of irreversible cracking that is present at all stress amplitudes, so that the reversible part decreases slightly in relative importance when the stress amplitude is decreased below 0.33. At a stress amplitude of 0.40 or above, the ratio of the reversible part of $\Delta R/R_o$ to the irreversible part of $\Delta R/R_o$ is much smaller than that at a stress amplitude below 0.40. This is due to the abrupt increase of the irreversible strain when the stress amplitude is increased from 0.33 to 0.40. As shown in Table 9, the irreversible strain is zero at stress amplitudes of 0.20 and 0.25, is essentially zero at a stress amplitude of 0.33, abruptly increases when the stress amplitude is increased from 0.33 to 0.40, and increases monotonically with increasing stress amplitude from 0.40 to 0.75. On the other hand, the reversible strain does not vary much with the stress amplitude. Table 9 shows good correlation between the irreversible strain and the irreversible part of $\Delta R/R_o$. Table 5 also shows significant effects of carbon fiber addition on mechanical properties, especially tensile and flexural properties.

To investigate the origin of the smart behavior rendered by the carbon fiber addition, the effect of the fiber addition on the fracture pattern was microscopically examined. Fig. 10 shows optical microscope photographs of the vertical edge surface of mortar cubes that had been compressed vertically on the horizontal surfaces up to about 70 percent of the fracture stress for (a) the mortar containing latex but no fibers, and (b) the mortar containing latex and 0.37 volume-percent fibers. As shown in Table 5, these two mortars have similar compressive strengths. The cracks are 1 μm in height in (b)

Table 9—Effect of stress amplitude in cyclic compressive loading on reversible and irreversible parts of $(\Delta R/R_o)/(\Delta R/R_o)_{fracture}$ and strain/strain$_{fracture}$ for mortar containing latex and 0.37 volume-percent carbon fibers

	$(\Delta R/R_o)/(\Delta R/R_o)_{fracture}$			Strain/strain$_{fracture}$		
Maximum stress / Fracture stress	Reversible	Irreversible	Reversible / Irreversible	Reversible	Irreversible	Reversible / Irreversible
0.75	0.039	0.244	0.16	0.29	0.44	0.66
0.65	0.037	0.102	0.36	0.29	0.33	0.88
0.50	0.032	0.115	0.28	0.38	0.12	3.17
0.40	0.0073	0.068	0.11	0.33	0.09	3.70
0.33	0.0034	0.0015	2.27	0.32	0.01	52.5
0.25	0.0025	0.0013	1.92	0.29	0.00	∞
0.20	0.0027	0.0017	1.59	0.27	0.00	∞

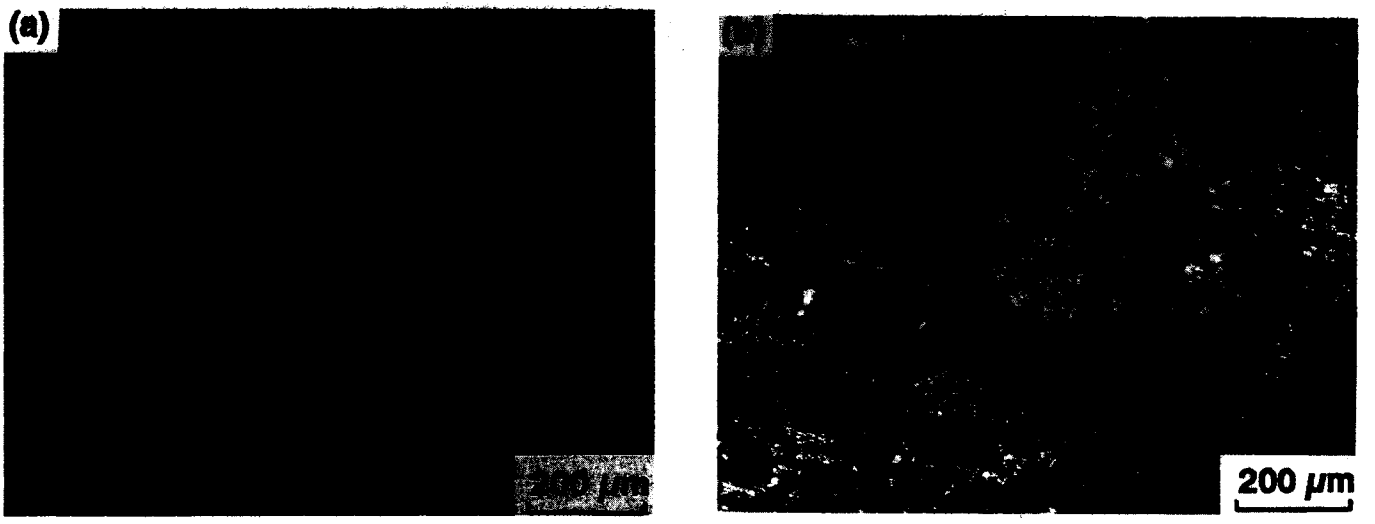

Fig. 10—Optical micrographs of cracks after compression to 70 percent of fracture stress of: (a) mortar containing latex; (b) mortar containing latex and 0.37 volume-percent fibers [crack height 100 μm in (a), 1 μm in (b); straight feature in middle of (b) is 10-μm-diameter fiber]

and 100 μm in (a), indicating that the fibers cause cracking control, which in turn results in the smart behavior.

When the carbon fibers in the latex-containing mortar were replaced by stainless steel fibers (60-μm-diameter, 5-mm-length, 6×10^{-5} Ω.cm electrical resistivity, in the amount of 0.37 volume-percent), an electrical response (Fig. 11) was observed during compressive deformation, though the plot of $\Delta R/R_o$ versus strain was more noisy than in the carbon fiber case (probably because of the large diameter of the steel fibers compared to the carbon fibers, as the steel fibers were much more conducting than the carbon fibers). However, when the carbon fibers were replaced by polyethylene fibers (38-μm-diameter, 5-mm-length, in the amount of 0.37 volume-percent), no electrical response was observed (Fig. 11). Thus, the electrically conducting nature of the fibers is necessary for observing the electrical response to elastic or inelastic deformation.

DISCUSSION

The origin of the concrete's ability to sense inelastic strain (i.e., damage) stems from the crack propagation associated with fracture and the fact that cracks are electrically insulating, thus increasing the electrical resistance of the concrete. In the absence of short fibers, the cracks in the concrete are large and catastrophically propagate, so that the electrical resistance increase on straining does not occur until right before fracture, at which the resistance increases abruptly (Fig. 7). However, in the presence of carbon fibers (in amounts as small as 0.2 volume-percent), the cracks in the concrete are orders of magnitude smaller in height (due to fiber bridging) and, in addition, conducting fiber breakage occurs during inelastic deformation, so that the resistance increases gradually with increasing strain until fracture and this resistance increase provides a measure of the strain (Fig. 4 under compression and Fig. 5 under tension). The ability of the concrete to sense reversible strain within the elastic regime (Fig. 8 under compression and Fig. 9 under tension) is related to the occurrence of reversible crack opening and closing (hence,

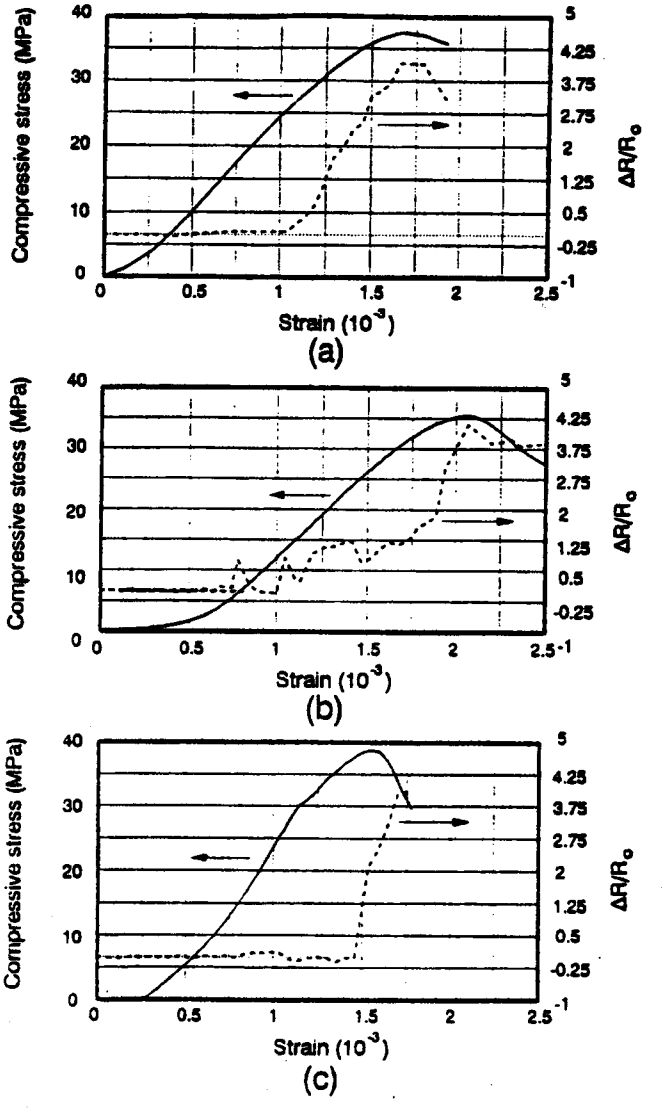

Fig. 11—Plots obtained simultaneously of compressive stress versus strain (solid curves) and of $\Delta R/R_o$ versus strain (dashed curves) up to fracture for mortars containing latex and 0.37 volume-percent fibers: (a) carbon fibers; (b) steel fibers; (c) polyethylene fibers

reversible resistance increase and decrease, respectively) due to fiber bridging, as explained below.

The sensing of both irreversible and reversible strain requires that the short fibers in the concrete be electrically conducting. As the fiber content needed is below the percolation threshold and the fractional resistance increase does not increase with increasing fiber content, the proximity between the fibers is not a factor; rather, the contact electrical resistance between the fiber and the matrix is an important factor in affecting the resistance measured. The volume fraction of cracks in the elastic regime is too low for the cracks alone to account for the resistance increase. Therefore, the reversible resistance change in the elastic regime under dynamic loading is attributed to the reversible change in the contact electrical resistance between the fiber and the matrix. The reversible change in the contact resistance is believed to be associated with the reversible fiber pullout of the bridging fiber across a crack. The fiber pullout accompanies crack opening (though slight, < 1 μm) and causes an increase in the electrical contact resistivity between the fiber and the matrix. The presence of fiber bridging is indicated by: 1) the decrease of the irreversible crack width after compressive loading (to 70 percent of the fracture stress) from 100 to 1 μm when the fibers are present; and 2) the large increases in tensile ductility and flexural toughness when the fibers are present. In the inelastic regime, fiber breakage and irreversible crack opening/propagation occur, thus causing irreversible resistance increase. That the conducting nature of the fibers is necessary for sensing in the inelastic regime prior to fracture means that the breaking of the conducting fibers (rather than the crack volume fraction increase) is the dominant cause for the irreversible resistance increase. However, at fracture, the crack volume fraction increase is the dominant cause for the irreversible resistance increase, so that the conducting nature of the fibers is not necessary for sensing at fracture.

As shown in Fig. 8 and 9, a part of the resistance change is reversible and a part is irreversible, even within the elastic regime, which is the case of Fig. 8 and 9. This is because the fiber-matrix interface weakening occurs irreversibly, even though the strain is totally reversible. The tensile and compressive strains at which this irreversible interface weakening occurs are respectively as low as 10^{-8} and 10^{-5}. The small values of these strains indicate the very high sensitivity of the strain sensing. As the stress amplitude increases, the irreversible portion becomes more important due to permanent flaw generation and it correlates with the irreversible strain, as shown in Table 9. Thus, the reversible and irreversible effects can be clearly distinguished. The combination of reversible and irreversible portions allows monitoring of the full range of dynamic loading, while the irreversible portion provides monitoring of the damage.

The fractional change in resistance at compressive fracture is higher when the fibers are used with methylcellulose and silica fume than when the fibers are used with methylcellulose alone, and is much higher than when the fibers are used with latex (Table 5). These differences are due to the differences in the degree of fiber dispersion, as indicated by the electrical resistivity (Table 4). The highest degree of fiber dispersion is obtained using methylcellulose + silica fume, as described in detail in a companion paper.[3]

CONCLUSION

1. Carbon fiber reinforced concrete was found to be an intrinsically smart concrete that can sense elastic deformation, inelastic deformation, and fracture, as shown under tension, compression, and flexure. The signal provided is the change in electrical resistance, which is reversible for elastic deformation and irreversible for inelastic deformation and fracture.

2. The presence of electrically conducting short fibers is necessary for the concrete to sense elastic or inelastic deformation, though the sensing of fracture does not require fibers.

3. The fibers serve to bridge the cracks and provide a conduction path. They do not need to touch one another.

4. The electrical resistance increase is due to conducting fiber pullout in the elastic regime, conducting fiber breakage in the inelastic regime, and crack propagation at fracture.

5. Within the elastic regime, irreversible damage was observed at strains as low as 10^{-8} under tension and 10^{-5} under compression, and is attributed to fiber-matrix interface weakening.

6. At the same fiber volume fraction, the presence of coarse aggregate decreases the fractional change in resistance as well as decreasing the electrical resistivity.

7. The fractional change in resistance at fracture is much higher under compression than tension due to the higher ductility under compression.

8. The fractional change in resistance at compressive fracture increases with increasing degree of fiber dispersion.

9. Applications include real-time damage assessment and dynamic load monitoring.

REFERENCES

1. Chen, Pu-Woei, and Chung, D. D. L., "Carbon Fiber Reinforced Concrete for Smart Structures Capable of Nondestructive Flaw Detection," *Smart Materials and Structures*, V. 2, 1993, pp. 22-30.

2. Chen, Pu-Woei, and Chung, D. D. L., "Concrete Reinforced with Up to 0.2 Volume-Percent of Short Carbon Fibers," *Composites*, V. 24, No. 1, 1993, pp. 33-52.

3. Chen, Pu-Woei; Fu, Xuli; and Chung, D. D. L., "Microstructural and Mechanical Effects of Latex, Methylcellulose, and Silica Fume on Carbon Fiber Reinforced Cement. " (in press)